Supplementary information for:

A juvenile Paleozoic ocean floor origin for eastern Stikinia, Canadian Cordillera

Ootes, L.[1], Milidragovic, D.[2], Friedman, R.[3], Wall, C.[3], Cordey, F.[4], Luo, Y.[5], Jones, G.O.[5], Pearson, D.G.[5], and Bergen, A.[6]
Luke.ootes@gov.bc.ca

BACKGROUND

In 2018, the British Columbia Geological Survey initiated a three-year mapping project in the Omineca Mountains of north-central British Columbia (Figs. 1, 2; Ootes et al., 2020a,b,c). Bedrock mapping was conducted from four-person camps for two weeks during the summer of 2019. Two factors led to mapping the Asitka Group and overlying units: 1) only brief descriptions exist in the literature and 2) geochronological and geochemical data were lacking.

FIELD RELATIONSHIPS

The field relationships are described in (Ootes et al., 2020a,b,c) and within the manuscript this supplementary information accompanies. The photographs (Figures S1-S6) support these observations and further catalogue the sample locations in this study.

ANALYTICAL TECHNIQUES

Igneous zircon U/Pb-Hf and trace element analysis

For igneous zircon analysis about 5 kg was sampled from unaltered and lichen-free bedrock. The analyses were completed at the Pacific Centre for Isotopic and Geochemical Research (PCIGR) at the University of British Columbia. Zircon was separated by standard techniques, hand picked in alcohol, and mounted in epoxy. Cathodoluminescence (CL) imaging

was carried out on a Philips XL-30 scanning electron microscope (SEM) equipped with a Bruker Quanta 200 energy-dispersion X-ray microanalysis system at the Electron Microbeam/X-Ray Diffraction Facility (EMXDF).

Zircon were initially analyzed by laser ablation inductively coupled mass spectrometry (LA-ICP-MS) to identify any grains with inheritance and to simultaneously collect trace element data (using the methods detailed in the online supplementary data). Analyses were conducted using a Resonetics RESOlution M-50-LR, which contains a Class I laser device equipped with a UV excimer laser source (Coherent COMPex Pro 110, 193 nm, pulse width of 4 ns) and a two-volume cell designed and developed by Laurin Technic Pty. Ltd. (Australia). The laser cell was connected via a Teflon squid to an Agilent 7700x quadrupole ICP-MS. A pre-ablation shot was used to ensure that the spot area on grain surface was contamination-free. Samples and reference materials were analyzed for 36 isotopes: ^{7}Li, ^{29}Si, ^{31}P, ^{43}Ca, ^{45}Sc, ^{49}Ti, Fe (^{56}Fe, ^{57}Fe), ^{89}Y, ^{91}Zr, ^{93}Nb, Mo (^{95}Mo, ^{98}Mo), ^{139}La, ^{140}Ce, ^{141}Pr, ^{146}Nd, ^{147}Sm, ^{153}Eu, ^{157}Gd, ^{159}Tb, ^{163}Dy, ^{165}Ho, ^{166}Er, ^{169}Tm, ^{172}Lu, ^{177}Hf, ^{181}Ta, ^{202}Hg, Pb (^{204}Pb, ^{206}Pb, ^{207}Pb, ^{208}Pb), ^{232}Th, and U (^{235}U, ^{238}U) with a dwell time of 0.02 seconds for each isotope. Pb/U and Pb/Pb ratios were determined on the same spots along with trace element concentration determinations. The settings included a spot size of 34 μm with a total ablation time of 30 seconds, frequency of 5 Hz, fluence of 5 J/cm2, power of 7.8 mJ after attenuation, pit depths of approximately 15 μm, He flow rate of 800 mL/min, N2 flow rate of 2 mL/min., and a carrier gas (Ar) flow rate of 0.57 L/min.

A subset of the best quality zircons was selected and analyzed by chemical abrasion isotope dilution thermal ionization mass spectrometry (CA-TIMS) by techniques modified from Mundil et al. (2004), Mattinson (2005), and Scoates and Friedman (2008), as outlined in the online supplementary methods. Isotopic ratios were measured with a single collector VG 54R

thermal ionization mass spectrometer equipped with analogue Daly photomultiplier. Analytical blanks are 0.1 pg for U and up 1.5 pg for Pb. Uranium fractionation was determined directly on individual runs using the EARTHTIME ET535 mixed $^{233-235}$U-^{205}Pb isotopic tracer (Schmitz and Schoene, 2007) and Pb isotopic ratios were corrected for fractionation of 0.25 ± 0.04%/amu. Zircon images and complete CA-TIMS analytical techniques are in Ootes et al. (2020c).

After CA-TIMS, four separate zircons from the same grain mount from sample A-rhy2 (19lo5-5) were selected for Lu-Hf analysis. For Lu-Hf analyses, zircon were selected on size, appropriate trace elements (e.g., low Ca, Fe, P, and La), and single zircon ^{206}Pb/^{238}U ages determined by LA-ICP-MS. Zircon were dissolved and after anion exchange by column chemistry and the Hf isotopic compositions were measured by static multicollection using a MC-ICP-MS (Nu Plasma II, NP 214) following the methods of Goolaerts et al. (2004) and Weis et al. (2007). Samples were run using a modified samples standard bracketing approach with JMC-475 Hf standard solution analyzed every second sample to monitor systematic in-run drift in the standard value. The average value of JMC-475 for the day of analysis was 0.282168 ± 6 (2SE; n=17). Initial ^{176}Hf/^{177}Hf and εHf values are calculated using λ^{176}Hf =1.867E-11 (Scherer et al., 2001; Söderlund et al., 2004), present day chondritic ^{176}Hf/^{177}Hf=0.282785, and ^{176}Lu/^{177}Hf =0.0336 (Bouvier et al., 2008). The Lu and Hf concentrations in the single zircon grains were determined by laser ablation.

Detrital zircon U/Pb-Hf and trace element analysis

For detrital zircon U-Pb and trace element analysis, about 5 kg was sampled from unaltered and lichen-free bedrock. At PCIGR, the samples were crushed and, following standard mineral separation, zircon separates were handpicked in alcohol and mounted in epoxy along

with reference materials. Cathodoluminescence (CL) imaging and LA-ICP-MS analyses were the same as those described above using a Resonetics RESOlution M-50-LR equipped with a UV excimer laser source connected to an Agilent 7700x quadrupole ICP-MS. Zircon images and complete analytical techniques are in Ootes et al. (2020c).

After detrital zircon U-Pb and trace element analyses, zircon grain mounts were sent to the Arctic Resources Laboratory at the University of Alberta for laser ablation-MC-ICP-MS Lu–Hf isotopic analysis. Full analytical details are in Ootes et al. (2020c) and reference material values for this analytical campaign are given in the online supplementary methods. Plešovice zircon was used as a primary reference material (Sláma et al., 2008). In this study we monitored the Yb interference correction, and the measured $^{176}Yb/^{173}Yb$ was iteratively calibrated to optimize the Yb-interference correction, monitored by zircon reference materials with variable Yb contents (91500, MUN1 and MUN3). Multiple analyses (n = 23) of the 91500 zircon standard (Blichert-Toft, 2008) yielded a weighted mean $^{176}Hf/^{177}Hf$ of 0.282313 ± 52 (2 SD). The results agree with the $^{176}Hf/^{177}Hf$ value of 0.282308 ± 6 (2 SD; Blichert-Toft, 2008). The mean $^{176}Hf/^{177}Hf$ for MUN1 and MUN3 (0.282135 ± 33 [2 SD], n = 42; 0.282130 ± 47 [2 SD], n = 33) are in good agreement with the solution MC-ICP-MS values of 0.282135 ± 31 (2 SD) for MUNZirc 1 and 3 (Fisher et al., 2011). The decay constant and parameters used for Hf model age calculations are $^{176}Hf/^{177}Hf$ (chondrite) = 0.0336, $^{176}Hf/^{177}Hf$ = 0.282785 (chondrite) after Bouvier et al. (2008) and $^{176}Hf/^{177}Hf$ (Depleted Mantle) = 0.038, $^{176}Hf/^{177}Hf$ = 0.283223 (Depleted Mantle) after Vervoort and Blichert-Toft (1999). Uncertainties on initial Hf ratios and epsilon Hf values were calculated using full error propagation, outlined by Ickert (2013). Data with unreasonable uncertainty were removed.

A second round of zircon U/Pb-Hf and trace element analysis was completed on 35 additional zircon grains from the same mineral separate of sample A-san1 (19lo14-5). The U-Pb and trace element analysis followed the same methods as above. Lutetium-Hafnium isotope analyses were completed on 32 of the zircons at PCIGR using a New Wave Research, 193nm laser ablation and a Nu Plasma (NP021) MC-ICP-MS. Data were reduced using Iolite 4 software (Paton et al., 2011) using the Hf Isotopes data reduction scheme (Woodhead et al., 2004). Uncertainties on initial Hf ratios were propagated through Iolite and epsilon Hf values were calculated using full error propagation, outlined by Ickert (2013). Reference materials used 91500 (Woodhead et al., 2005) as a primary reference and Plešovice – average $^{176}Hf/^{177}Hf$ age = 0.282485 ± 0.000065 (n = 5), Temora2 – average $^{176}Hf/^{177}Hf$ age = 0.282669 ± 0.000055 (n = 5), GJ1 – average $^{176}Hf/^{177}Hf$ age = 0.282005 ± 0.000049 (n = 5), FC1 – average $^{176}Hf/^{177}Hf$ age = 0.282152 ± 0.000037 (n = 5) were used as validation.

References

Blichert-Toft, J., 2008, The Hf isotopic composition of zircon reference material 91500: Chemical Geology, v, 253, p. 252-257.

Bouvier, A., Vervoort, J.D., and Patchett, J.P., 2008, The Lu–Hf and Sm–Nd isotopic composition of CHUR: Constraints from unequilibrated chondrites and implications for the bulk composition of terrestrial planets: Earth and Planetary Science Letters, v. 273, p. 48-57.

Elia, E.A., and Ferbey, T., 2020, Generating photogrammetric DEMs in the field from remotely piloted aircraft systems, *in* Geological Fieldwork 2019: British Columbia Ministry of Energy, Mines and Petroleum Resources, British Columbia Geological Survey Paper 2020-01, p. 189-200.

Fisher, C.M., Hanchar, J.M., Samson, S.D., Dhuime, B., Blichert-Toft, J., Vervoort, J.D., and Lam, R., 2011, Synthetic zircon doped with hafnium and rare earth elements: A reference material for in situ hafnium isotope analysis: Chemical Geology, v. 286, p. 32-47.

Goolaerts, A., Mattielli, N., De Jong, J.T.M., Weis, D., and Scoates, J., 2004, Hf and Lu isotopic reference values for the zircon standard 91500 by MC-ICP-MS: Chemical Geology, v. 206, p. 1-9.

Ickert, R.B., 2013, Algorithms for estimating uncertainties in initial radiogenic isotope ratios and model ages: Chemical Geology, v. 340, p. 131-138.

Ludwig, K. R., 2003, Isoplot 3.00, A Geochronological Toolkit for Microsoft Excel: University of California at Berkeley.

Mattinson, J.M., 2005, Zircon U-Pb chemical abrasion ("CA-TIMS") method: Combined annealing and multi-step partial dissolution analysis for improved precision and accuracy of zircon ages: Chemical Geology, v. 220, p. 47-66.

Mundil, R., Ludwig, K. R., Metcalfe, I., and Renne, P. R., 2004, Age and timing of the Permian mass extinctions: U/Pb dating of closed-system zircons: Science, v. 305, p. 1760-1763.

Ootes, L., Bergen, A.L., Milidragovic, D., and Jones, G.O., 2020a, Bedrock geology of the northern Hogem batholith and its surroundings, north-central British Columbia: British Columbia Ministry of Energy and Mines and Petroleum Resources, British Columbia Geological Survey Open File 2020-02, scale 1:50,000.

Ootes, L., Bergen, A.L., Milidragovic, D., Jones, G.O., Camacho, A., and Friedman, R., 2020b, An update on the geology of northern Hogem batholith and its surroundings, north-central British Columbia, *in* Geological Fieldwork 2019: British Columbia Ministry of Energy, Mines and Petroleum Resources, British Columbia Geological Survey Paper 2020-01, p. 25-47.

Ootes, L., Jones, G., Schiarizza, P., Milidragovic, D., Friedman, R., Camacho, A., Luo, Y., Vezinet, A., Pearson, D.G., and Zhang, S., 2020c, Geochronologic and geochemical data from northern Hogem batholith and its surroundings, north-central British Columbia: British Columbia Ministry of Energy, Mines and Petroleum Resources, British Columbia Geological Survey Geofile 2020-01, 25 p.; digital files.

Paton, C., Hellstrom, J., Paul, B.,Woodhead, J. and Hergt, J., 2011, Iolite: Freeware for the visualisation and processing of mass spectrometric data: Journal of Analytical Atomic Spectrometry, v. 26, p. 2508-2518. doi:10.1039/c1ja10172b.

Scherer, E.E., Münker, C., and Mezger, K., 2001, Calibration of the Lutetium–Hafnium clock: Science**, v.** 293, p. 683-687.

Schmitz, M.D., and Schoene, B., 2007, Derivation of isotope ratios, errors, and error correlations for U-Pb geochronology using ^{205}Pb-^{235}U-(^{233}U)-spiked isotope dilution thermal ionization mass spectrometric data: Geochemistry, Geophysics, Geosystems, v. 8, doi:10.1029/2006GC001492.

Scoates, J.S., and Friedman, R.M. 2008, Precise age of the platinuferous Merensky Reef, Bushveld Complex, South Africa, by the U-Pb ID-TIMS chemical abrasion ID-TIMS technique: Economic Geology, v. 103, p. 465-471.

Sláma, J., Košler, J., Condon, D.J., Crowley, J.L., Gerdes, A., Hanchar, J.M., Horstwood, M.S. A., Morris, G.A., Nasdala, L., Norberg, N., Schaltegger, U., Schoene, B., Tubrett, M.N., and Whitehouse, M.J., 2008, Plešovice zircon - A new natural reference material for U-Pb and Hf isotopic microanalysis: Chemical Geology, v. 249, p. 1-35.

Söderlund, U., Patchett, P.J., Vervoort, J.D., Isachsen, C.E., 2004, The ^{176}Lu decay constant determined by Lu–Hf and U–Pb isotope systematics of Precambrian mafic intrusions: Earth and Planetary Science Letters, v. 219, p. 311-324.

Vervoort, J.D., and Blichert-Toft, J., 1999, Evolution of the depleted mantle: Hf isotope evidence from juvenile rocks through time: Geochimica et Cosmochimica Acta, v. 63, p. 533–556.

Weis, D., Kieffer, B., Hanano, D., Barling, J., Pretorius, W., Maerschalk, C. and Mattielli, M., 2007, Hf isotope compositions of US Geological Survey reference materials: Geochemistry, Geophysics, Geosystems, v. 8, Q06006, doi:10.1029/2006GC001473.

Woodhead, J.D., and Hergt, J.M., 2005, A preliminary appraisal of seven natural zircon reference materials for in situ Hf isotope determination: Geostandards and Geoanalytical Research, v. 29.2, p. 183-195.

Woodhead, J., Hergt, J., Shelley, M., Eggins, S., and Kemp, R., 2004, Zircon Hf-isotope analysis with an excimer laser, depth profiling, ablation of complex geometries, and concomitant age estimation: Chemical Geology, v. 209, p. 121-135.

SUPPLEMENTARY FIGURES

Figure S1. Outcrop photographs of the Asitka Group at location 1. A) Relationship between basaltic andesite, rhyolite, slate, and red chert. B) Rhyolite (A-rhy1) sample location. C) Sample of radiolarian-bearing chert (red) with interbedded mudstone (brown).

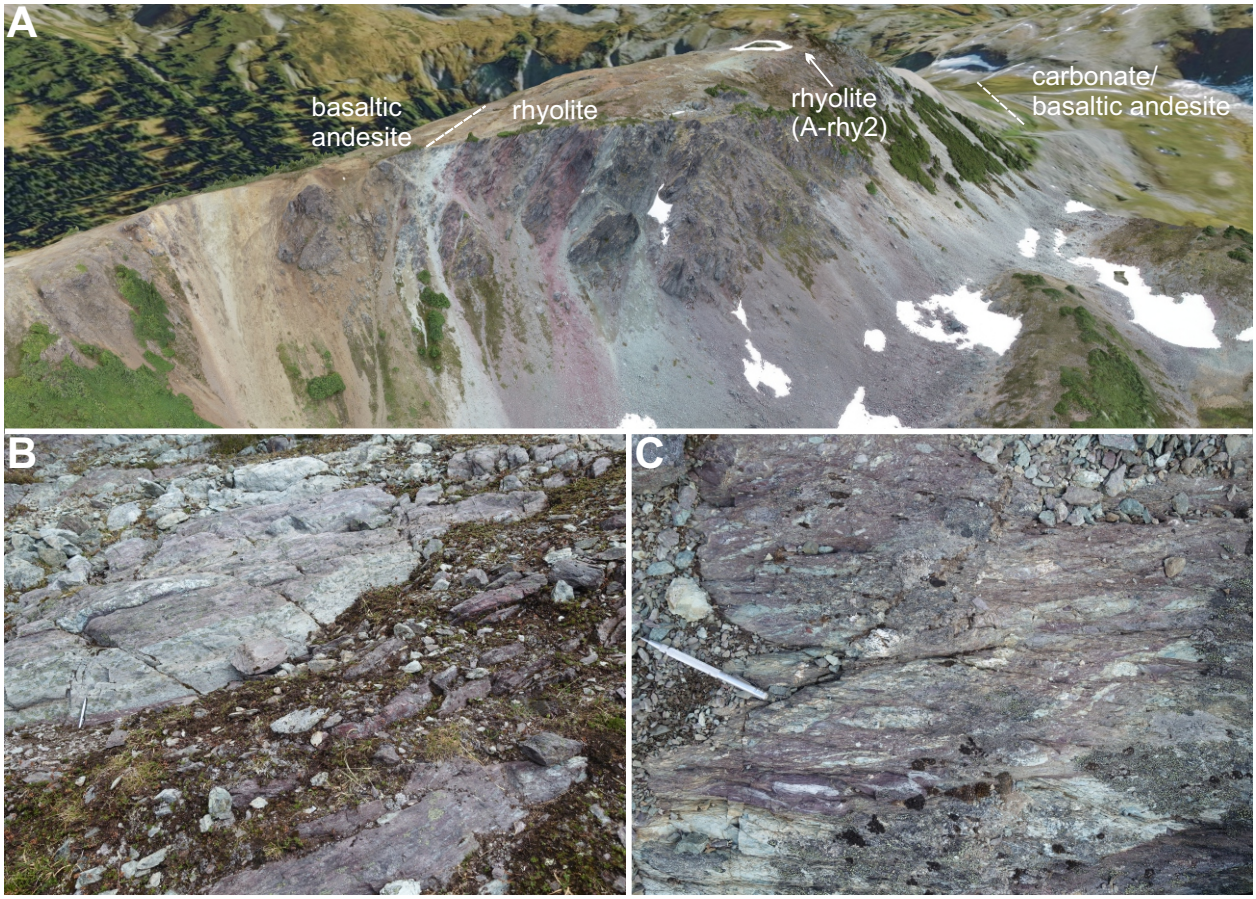

Figure S2. A) The Asitka Group at location 2. A) Perspective view toward the southwest of the ridge where rhyolite sample (A-rhy2) was collected. This 3-dimensional high-resolution model, positioned over Mapbox Satellite global base map imagery, was generated from remotely piloted aircraft imagery and structure-from-motion photogrammetry techniques (see Elia and Ferbey (2020) for details). B) Alternating white and pink fragmental rhyolite. C) Strongly deformed pink and white fragmental rhyolite with volcanic clasts. Sample A-rhy2 was collected from a similar lithology.

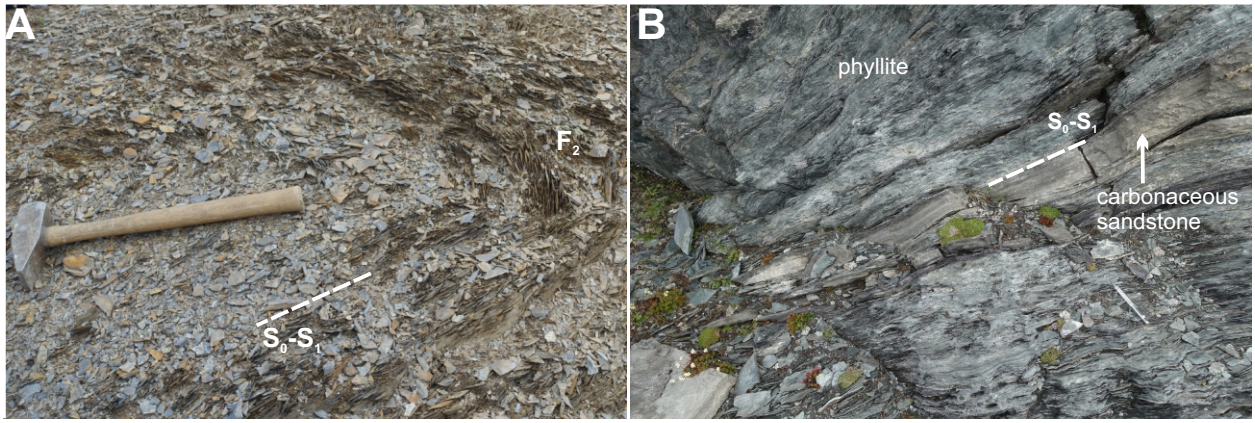

Figure S3. The Asitka Group at location 3. A) Dark grey folded mudstone (F_2). Bedding (S_0) and first generation foliation (S_1) are parallel. B) Strongly deformed phyllite with interbed of arbonaceous sandstone.

Figure S4. The Takla Group (Dewar Formation). A) Basal black graphitic mudstone from the southeast of location 3. B) Typical interbedded siltstone (grey) and slates (recessive, dark brown). Individual beds are up to 2-4 cm thick and bedsets are 10-15 m thick. View is toward the north. C) From top to bottom: (1) monomictic conglomerate with coarse-grained volcanic-derived plagioclase-rich pebbles; (2) green and grey argillite with planar laminations; and (3) sandstone with volcanic-derived plagioclase-rich pebbles, scour structure (middle) and weakly defined cross-beds. E) Conglomerate with volcanic-derived plagioclase-rich pebbles and a sub-angular carbonate clast (grey, recessive weathering). The carbonate clast is interpreted to have been derived from the underlying Asitka Group. Scribe (circled) for scale.

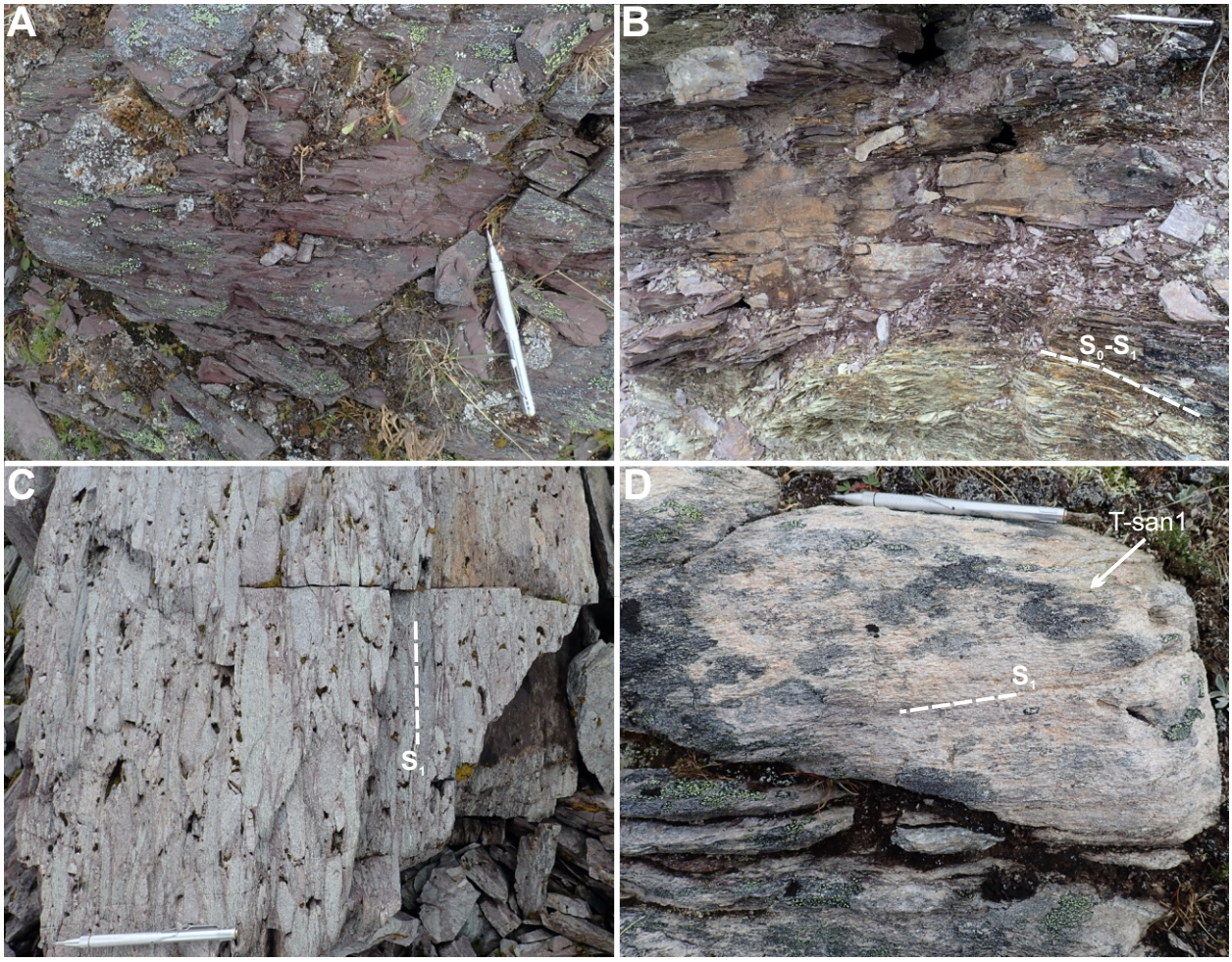

Figure S5. The Hazelton Group (Telkwa Formation). A) Red mudstone with a moderate to strong foliation. B) Interbedded red and green mudstone with first generation foliation (S_1) parallel to bedding. C) Monomictic conglomerate with a pink sandstone matrix; S_1 foliation is defined by aligned white volcanic-derived plagioclase-rich clasts. D) Pink to white weathered medium-grained sandstone. This is the location of Telkwa Formation sandstone sample (T-san1).

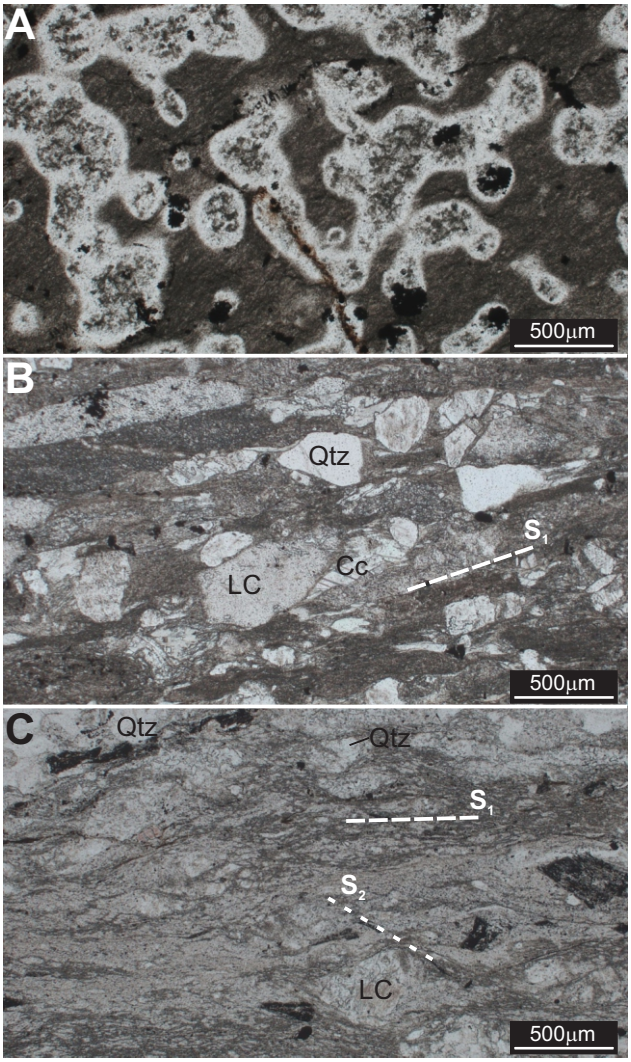

Figure S6. A) Devitrified spherulite-like features in Asitka Group rhyolite sample (A-rhy1). Plane polarized light. B) Quartz (Qtz) and lithic clasts (LC) in Asitka Group sandstone sample (A-san1). Penetrative S_1 foliation from lower left to upper right in the matrix and as defined by aligned sand grains. C) Quartz and lithic clasts in Telkwa Formation sandstone sample (T-san1). Most of the matrix is fine-grained quartz and mica. A strong deformation fabric (S_1) is weakly crenulated (S_2).

Figure S7. Zircon trace element screening results. Red symbols are Asikta Group and green symbols are Telkwa Formation detrital zircons. Symbols that are grey '+' are Asitka Group and 'x' are Telkwa Formation zircons that have trace element compositions that indicate a mineral inclusion (e.g., apatite, titanite) was intercepted during laser ablation. These data have been removed. A-E) $^{206}Pb/^{238}U$ (age) versus trace element. F) La versus Ce.

A)

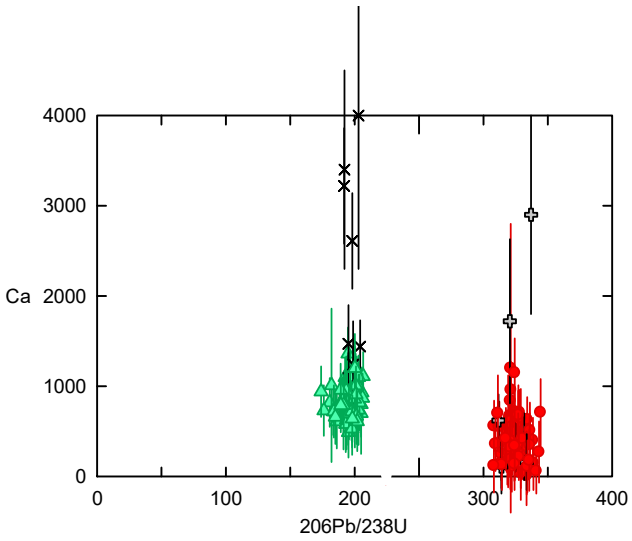

B)

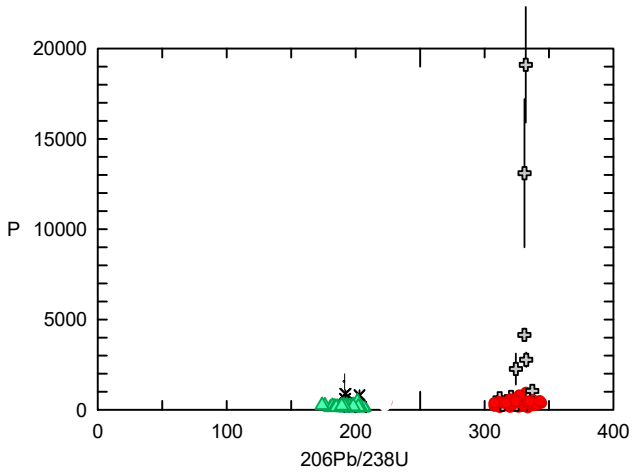

C)

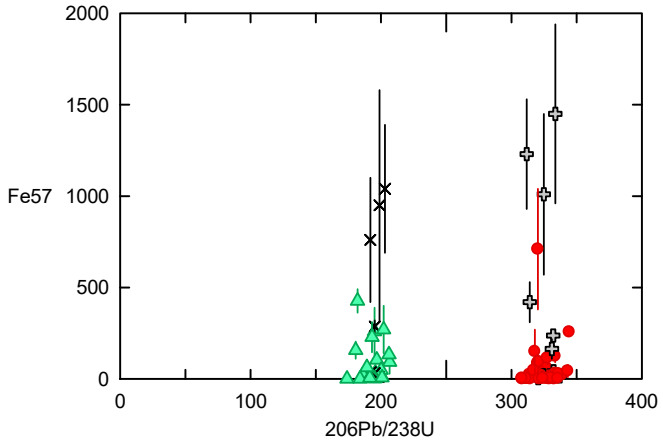
2000
1500
Fe57 1000
500
0
0
100
200
300
400
206Pb/238U

D)

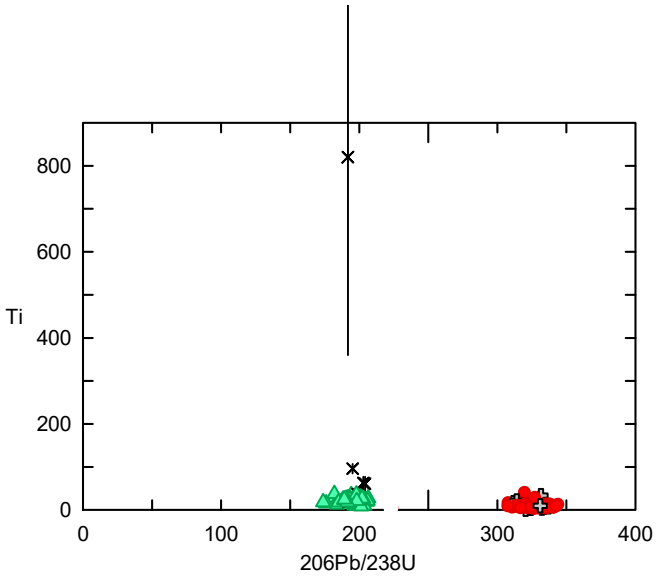
800
600
Ti
400
200
0
0
100
200
300
400
206Pb/238U

E)

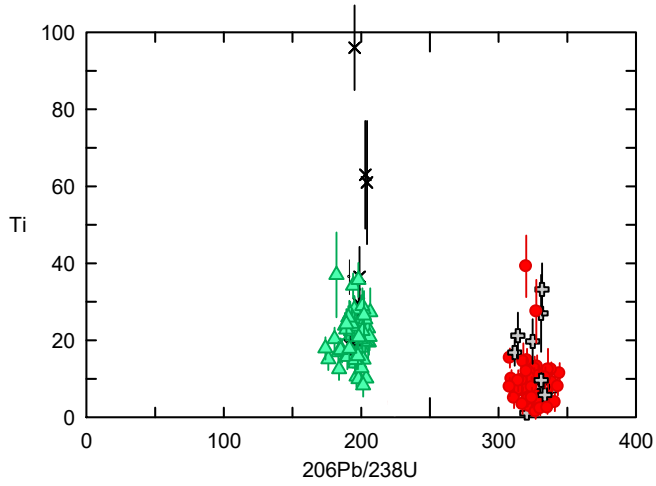
100
80
60
Ti
40
20
0
0
100
200
300
400
206Pb/238U

F)

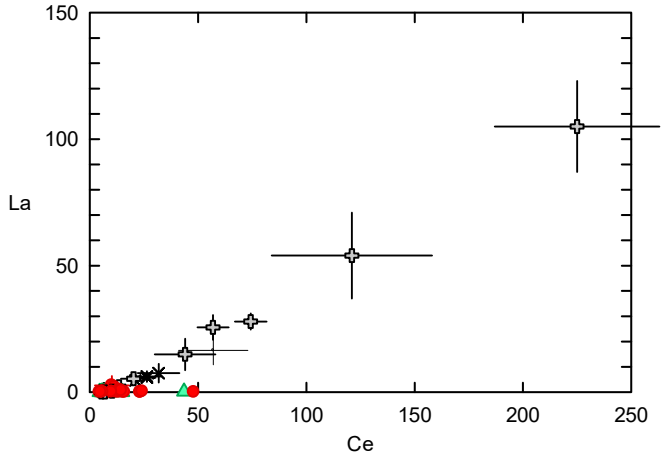

Figure S8. Asitka Group sample A-rhy2 igneous zircon Hf results from MC-ICP-MS.

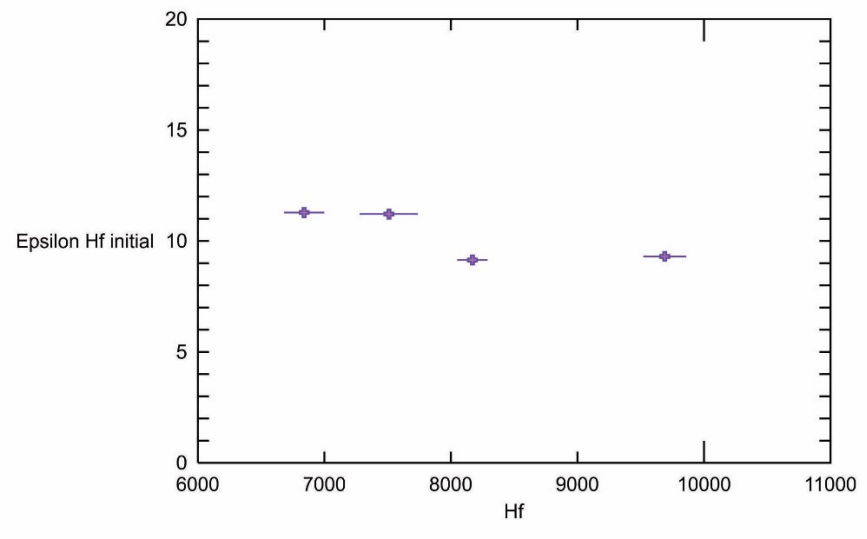

Figure S9. Asitka Group sample A-san1 (19lo14-5a) detrital zircon results, plotted using Isoplot (Ludwig, 2003). A) Probability-histogram (n=91), B) youngest statistical population (YSP), and C) result using tuffzirc application.

A)

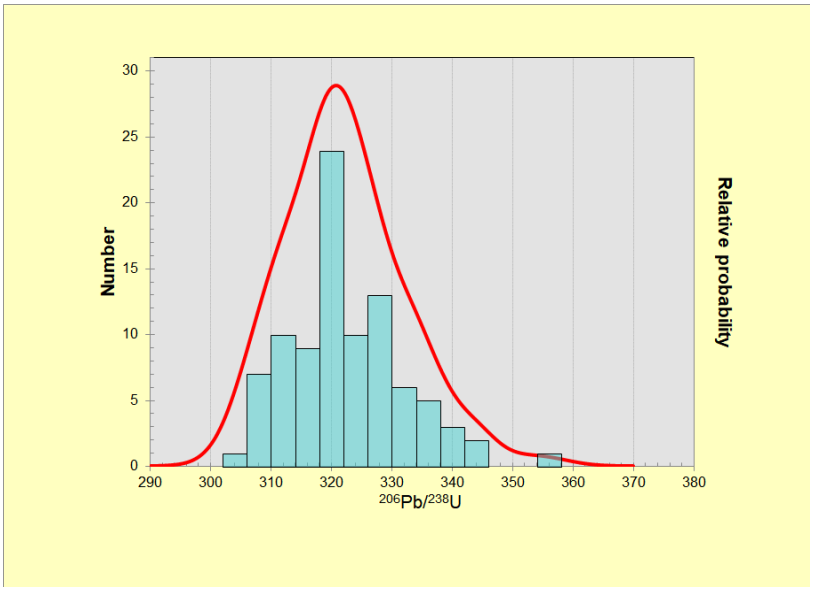

B)

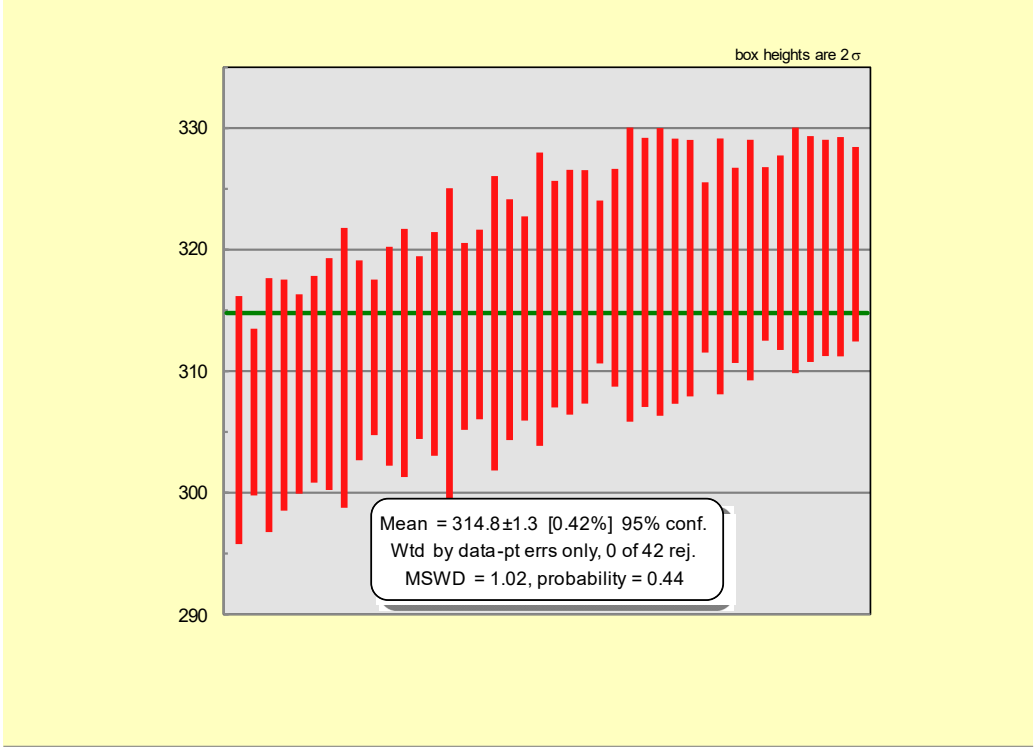

C)

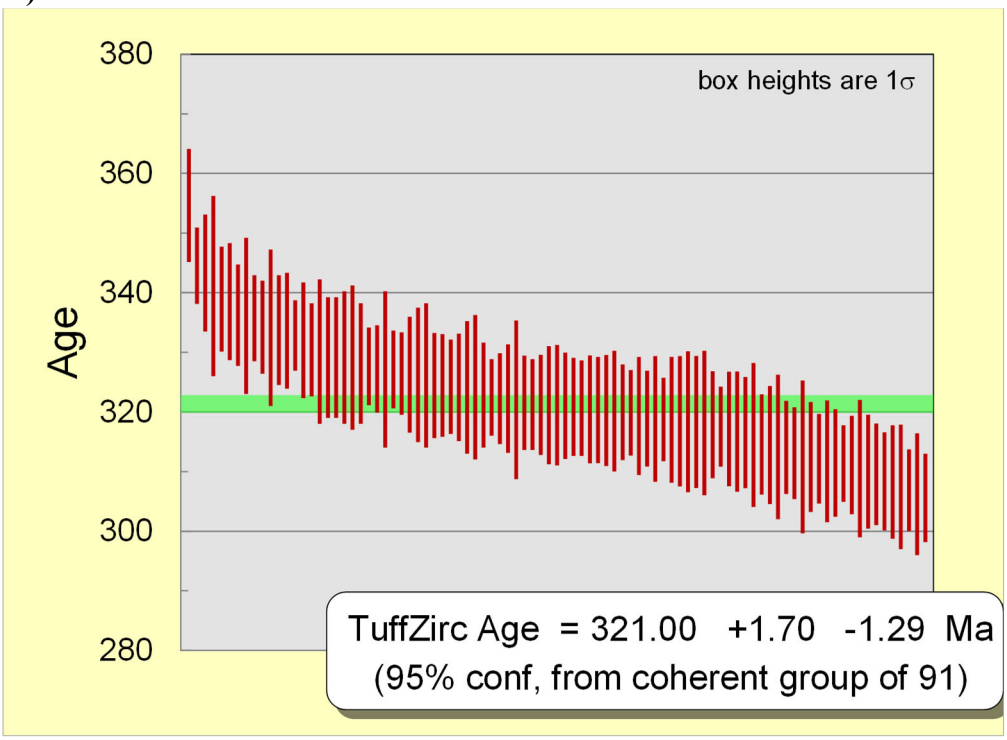
380
360
340
320
300
280
Age
box heights are 1σ
TuffZirc Age = 321.00 +1.70 -1.29 Ma
(95% conf, from coherent group of 91)

Figure S10. Telkwa Formation sample T-san1 (19GJ18-3) detrital zircon results, plotted using Isoplot (Ludwig, 2003). A) Probability-histogram (n=62), B) youngest statistical population (YSP), C) result using tuffzirc application, D) two component unmixing; results of three component unmixing is included in the manuscript.

A)

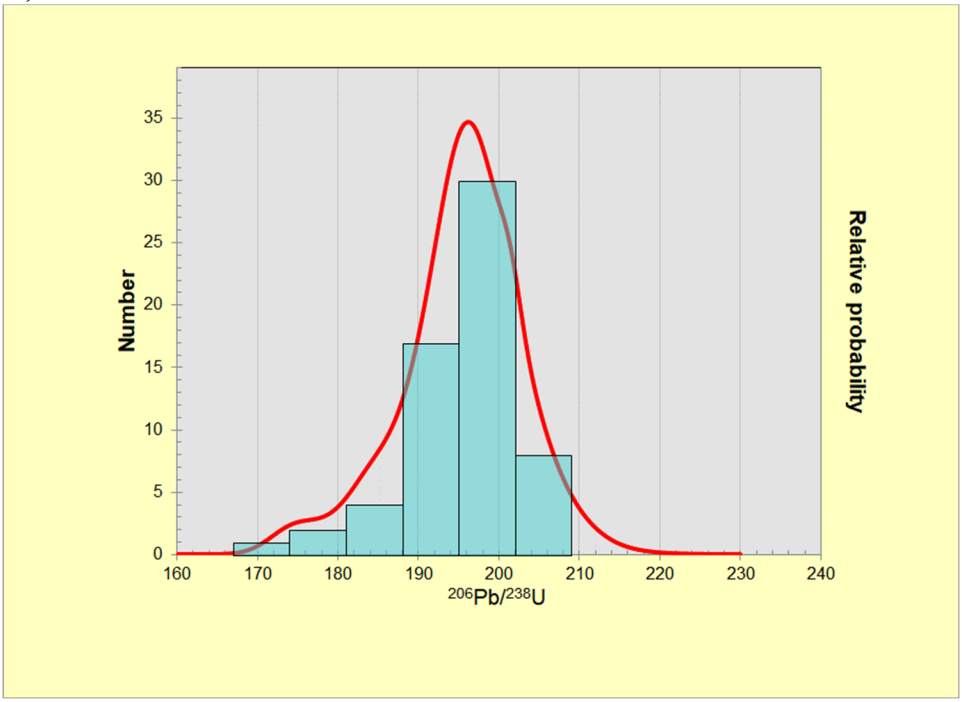

B)

C)

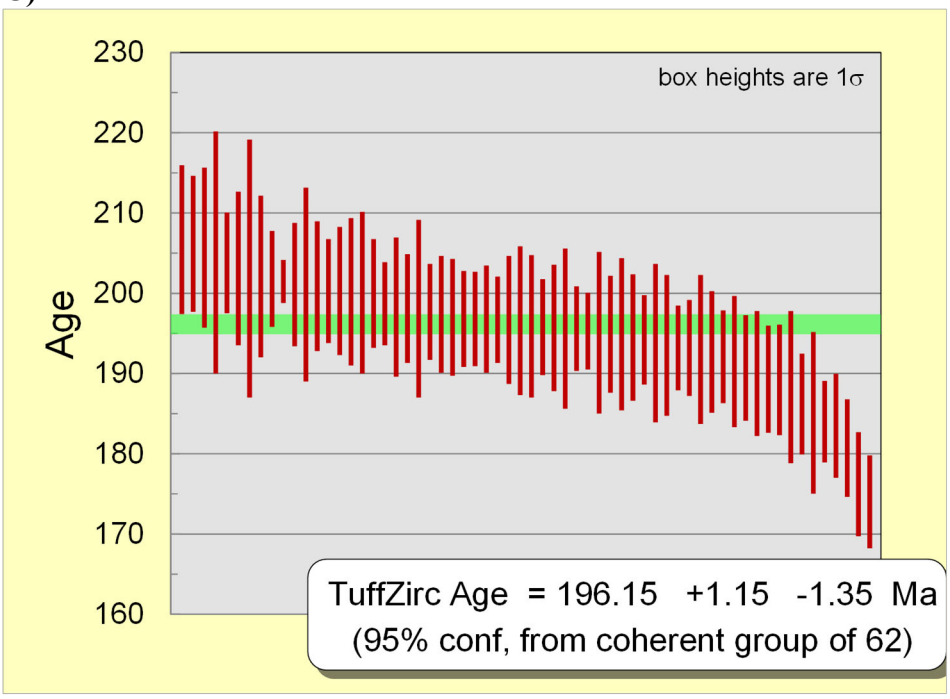

D)

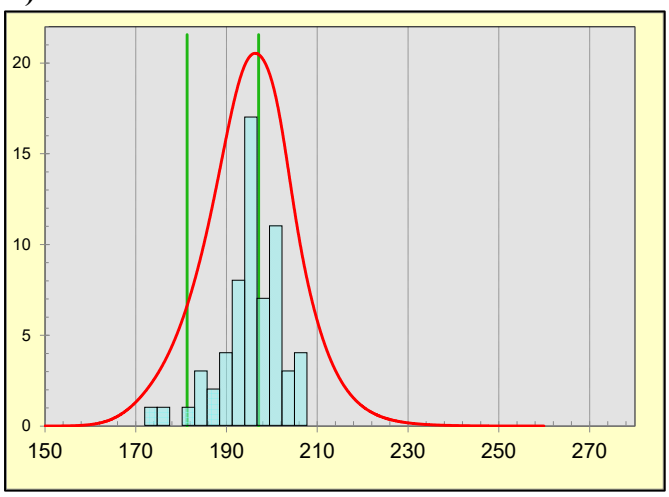

Age	±2s	fraction	±2s
181.3	2.7	0.12	0.09
197.09	0.96	0.88	---

relative misfit = 0.770

Sigma-Rho Matrix

	f1	t1	t2
f1	0.047	0.190	0.105
t1	0.190	1.36	0.143
t2	0.105	0.143	.48

Figure S11. Zircon chemistry from sample A-rhy1 (yellow), A-rhy2 (purple), A-san1 (red), T-san1 (green). Red stars are Paleoproterozoic zircon from A-san1. Error bars are 2σ.

A)

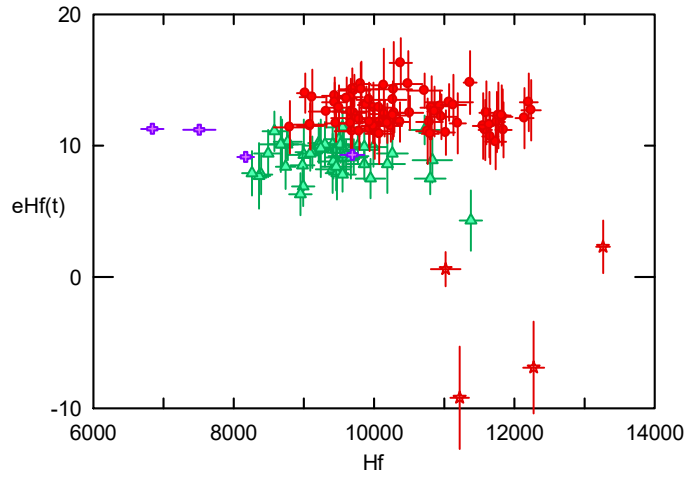

B)

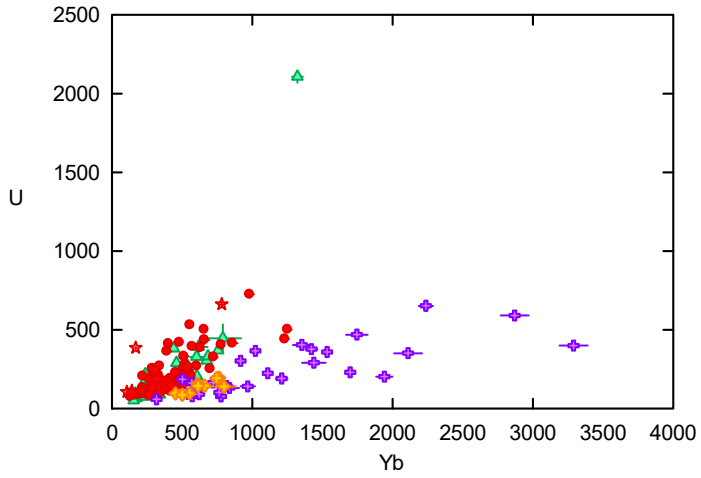

C)

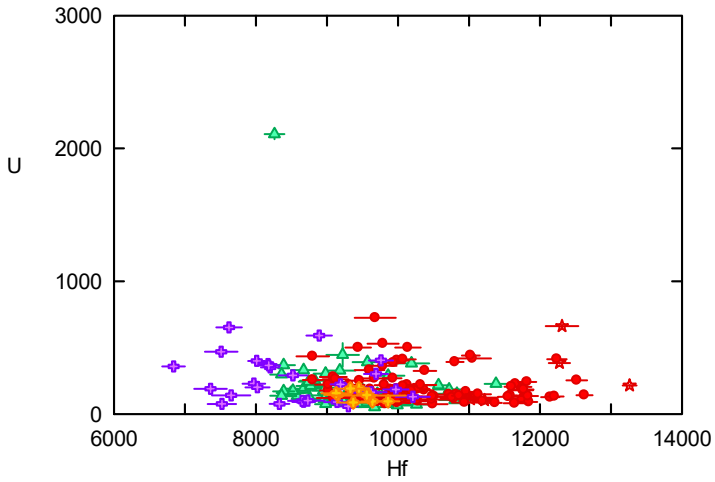

D)

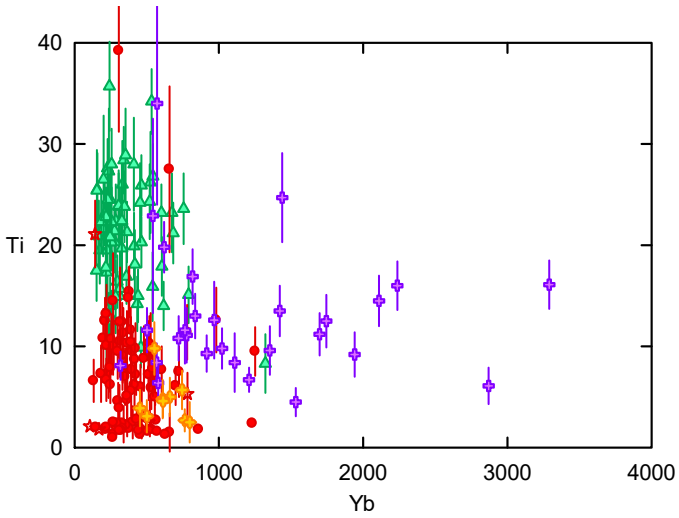
Ti
Yb
0
10
20
30
40
0
1000
2000
3000
4000

E)

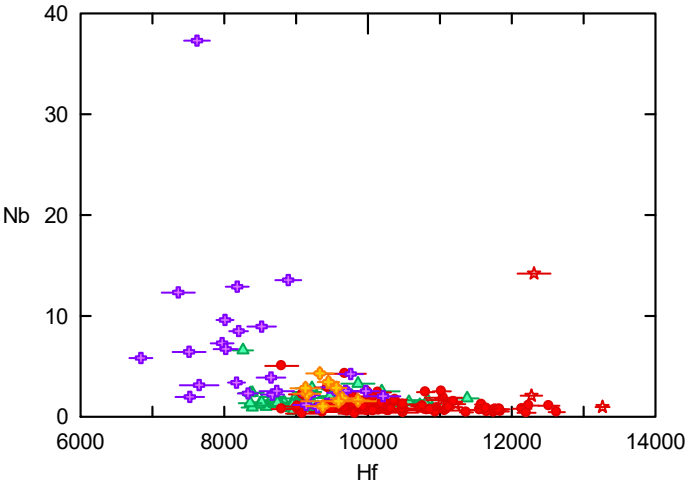
Nb
Hf
0
10
20
30
40
6000
8000
10000
12000
14000

F)

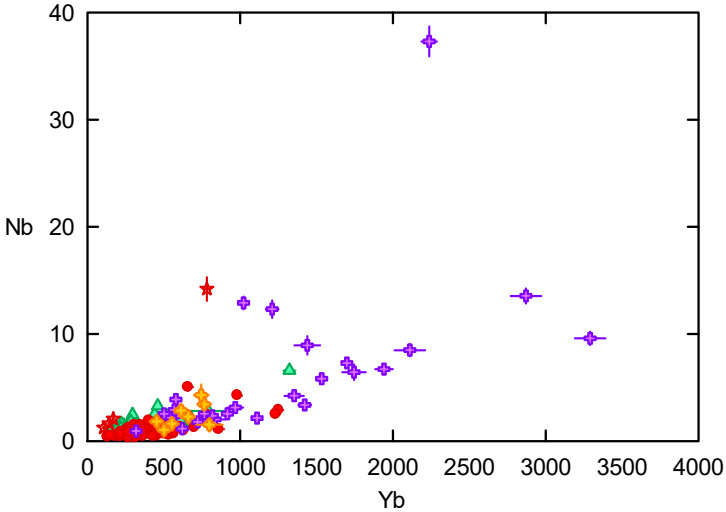
Nb
Yb
0
10
20
30
40
0
500
1000
1500
2000
2500
3000
3500
4000

G)

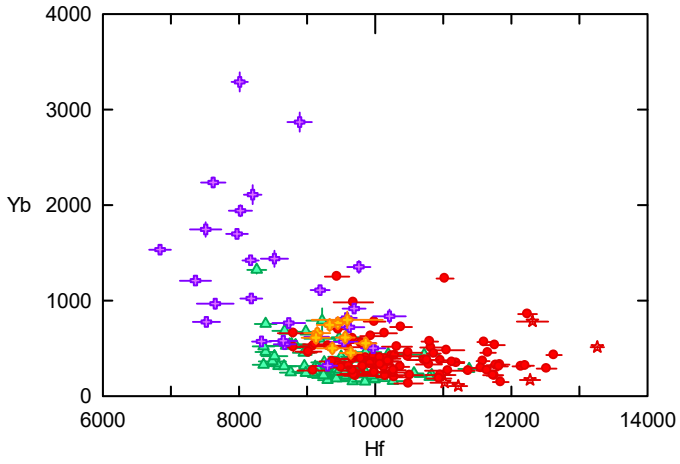
4000
3000
Yb 2000
1000
0
6000
8000
10000
12000
14000
Hf

H)

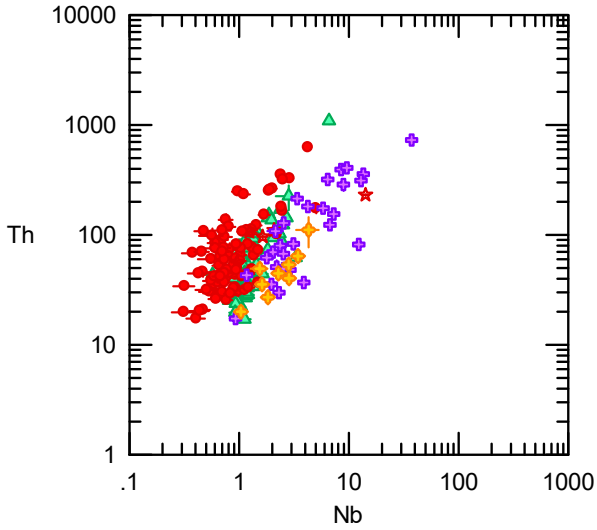
10000
1000
Th 100
10
1
.1
1
10
100
1000
Nb

I)

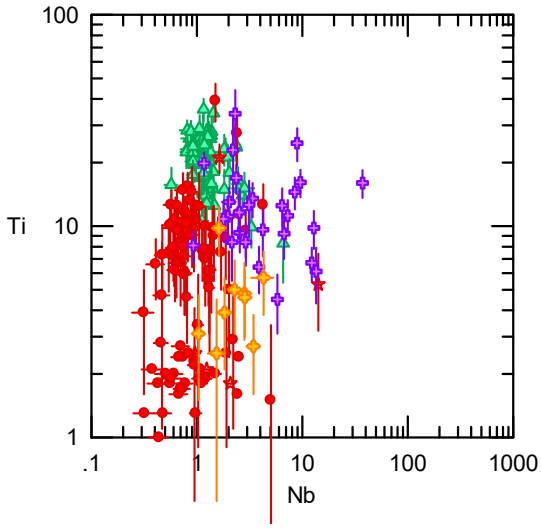
100
Ti 10
1
.1
1
10
100
1000
Nb

J)